Journal of Geochemical Exploration xxx (2012) xxx–xxx

Contents lists available at SciVerse ScienceDirect

Journal of Geochemical Exploration

journal homepage: www.elsevier.com/locate/jgeoexp

Au and Cr mobilization through metasomatism: Microchemical evidence from ore-bearing listvenite, South Eastern Desert of Egypt

Ashraf Emam [a,*], Basem Zoheir [b]

[a] Goology Department, Faculty of Science, Aswan University, Aswan 81528, Egypt
[b] Geology Department, Faculty of Science, Benha University, Benha 13518, Egypt

ARTICLE INFO

Article history:
Received 14 June 2012
Accepted 3 November 2012
Available online xxxx

Keywords:
Listvenite
Lode-gold
Element mobilization
Metasomatism
Haimur deposit
Egypt

ABSTRACT

Listvenite is an uncommon rusty-red-weathering quartz-fuchsite-carbonate rock formed by the metasomatic transformation of mafic and ultramafic rocks, typically at the margins of fault-bound ophiolitic blocks. In the highly deformed orogenic belts, listvenite is commonly associated with metal enrichments and auriferous quartz veins. Electron microprobe measurements are used to study the mobility and dispersion of Cr, Au and other elements in listvenite associate with the Haimur gold deposit, South Eastern Desert of Egypt. The results suggest that the Cr-Fe^{3+}-enriched spinel rims and Cr-chlorite aureoles around relict Cr-rich cores are the result of destabilization of chromite during metasomatism. The association of disseminated Cr-chlorite, fuchsite and Fe-Mg carbonate in silicified wallrock and slivers within the auriferous quartz lodes implies Cr mobilization by CO_2-rich hydrothermal fluids. Intergrowth textures suggest that listvenitization was concomitant with quartz veining.

Early paragenetic idiomorphic Co-gersdorffite crystals disseminated in the quartz lodes show similar compositions, generally containing several hundreds ppm Au, while dispersed, irregular gersdorffite grains, Ni-bearing arsenopyrite and As-bearing pyrite are considered relatively late. These late paragenetic sulfarsenide minerals commonly contain up to 2000 ppm Au, and less common Sb. The distribution of Ni, Co, As, and Au in these minerals suggests mobilization and re-distribution by infiltrating hydrothermal fluids with sufficient CO_2 to form the abundant carbonate in lodes and wallrocks. The positive correlation between Ni and As in the disseminated pyrite and arsenopyrite argues for the dissolution of Ni-bearing phases in serpentinite during carbonatization and co-precipitation.

Temperature estimates based on the composition of gersdorffite, arsenopyrite and hydrothermal chlorite reflect the development of the observed mineral associations as the system cooled down from ~450 to 250 °C. The oxygen and sulfur fugacity ($\log fO_2 = -30$ and $\log fS_2 = -8$ bars at 350–400 °C) corresponds to the low sulfidation and oxidizing environment typical for orogenic, silica-rich ore-bearing listvenite.

1. Introduction

Listvenite is a term used in Russian and Eastern European literature to describe distinctive, carbonatized serpentinite, composed mainly of fuchsite, Mg-Ca carbonates, quartz, talc and minor serpentine, chlorite, Fe-oxides, Ni-Fe-Co-sulfides and arsenides (e.g., Halls and Zhao, 1995; Plissart and Féménias, 2009). The geological interest of such rocks is linked to their associated metal enrichment (Au, Co, Sb, Cu and Ni; Buisson and Leblanc, 1985; Hansen et al., 2005; Nixon, 1990; Uçurum, 2000). The association of auriferous lodes with listvenite has been observed in the greenstone belts of the Eastern Desert of Egypt, where it is commonly associated with sheared serpentinite at fault intersections or along basal detachment (décollement) of major thrust structures, especially where granitoid massifs and stocks occur, e.g., the Barramiya and El-Anbat gold deposits (Zoheir, 2011; Zoheir and Lehmann, 2011). Significant gold concentrations in listvenite and listvenitized serpentinite have been reported in several areas in the Egyptian Eastern desert (e.g., Botros, 1993; El-Dougdoug, 1990; El-Mezayen et al., 1995; Hassaan et al., 1996, 2009; Osman, 1995; Ramadan, 2002; Ramadan et al., 2005).

Listvenitization of ultramafic rocks is commonly attributed to emplacement of orogenic granitoids that produced chloride–carbon dioxide fluids (e.g., Auclair et al., 1993; Sazanov, 1975). The anomalous concentrations of Cr, Ni, Co, and Pt in listvenites attests to the ultramafic protolith and reveal mobility of these elements throughout metasomatism (e.g., Molchanov et al., 2000, 2006). Leblanc and Fischer (1990) inferred that the ultramafic rocks are the source for Co and Au which are mobilized from the primary magmatic sulfide species during serpentinization.

Apart from 'visible' gold, finely dispersed and colloidal gold of less than 1 μm particles size is known in several deposits. This gold is most often contained in chalcedony-type quartz and early 'magmatic' sulfides (e.g., Kovalenker et al., 1986; Nekrasov et al., 1988). In this

* Corresponding author. Fax: +20 793480450.
E-mail address: ashrafemam99@hotmail.com (A. Emam).

0375-6742/$ – see front matter © 2012 Elsevier B.V. All rights reserved.
http://dx.doi.org/10.1016/j.gexplo.2012.11.004

context, accurate characterization of gold ores and element mobility and re-distribution can be attained by high resolution analytical techniques. In the present work, high-resolution electron microprobe measurements are used to study the mobility and dispersion of metals during metasomatism of the ultramafic rocks in Haimur gold deposit.

2. Methodology

Petrographic examination and preliminary mineral identification were done on polished and thin sections using a Zeiss Axion microscope, and aided by SEM back-scattered electron imaging. Mineral chemistry of selected magmatic and hydrothermal mineral phases is intended to reveal more information about gold genesis based on mineral composition and paragenesis. Mineral microchemical compositions were obtained with a Cameca SX100 four spectrometer, fully automated electron microprobe using a wavelength-dispersive X-ray spectrometry at TU-Clausthal, Germany.

For trace element analysis the wavelength dispersive spectroscopy (WDS) method was used. To get low detection limits, the microprobe was operated at high probe currents and accelerating voltages over long measuring (e.g., Kojonen and Johanson, 1999; Ziebold, 1967). Therefore, analyses of sulfide minerals were made at 30 keV accelerating voltage and 40 nA (and 300 nA for Au, Sb, Ag, Ni, Co) beam current, and counting times of 10 to 300 s, using a 2 μm beam diameter. Carbonate minerals, fuchsite and chlorite were analyzed under operating conditions of 15 kV, 20 ηA beam current and a 5 μm beam diameter. Relative accuracy of the analyses, based upon comparison between measured and published compositions of standard reference materials, is ~1–2% for concentrations above 1 wt.% and ~5–10% for concentrations below 1 wt.%. Element detection limits (wt.%) at the three sigma level were As (0.02), Cd (0.03), Co (0.01), Cu (0.02), Fe (0.01), Mn (0.01), Pb (0.15), S (0.02), Ni (0.01), Sb (0.02), V (0.01), Au (0.006), Ag (0.01) and Zn (0.03).

3. Gold mineralization: setting and characteristics

The Wadi Allaqi district, in the South Eastern Desert of Egypt, has a long history of gold mining dating back to the Dynastic times. Evidence of the historical mining activity is clearly seen in stoped out quartz veins at shallow depths by means of shafts and adits and the presence of numerous stone tools used in crushing the gold ore. The area contains more than 12 gold occurrences most of which are hosted in Precambrian metavolcanic and metasedimentary rocks or in placers apparently derived from these rocks (Gabra, 1986). Klemm et al. (2001) and Kusky and Ramadan (2002) suggested that gold–quartz veins of the Wadi Allaqi region are generally structurally-controlled, and are genetically related to altered ultramafic rocks associated with imbricate thrust faults, or to shear zones truncating the thrust slices (e.g., El-Shimi, 1996; Zoheir, 2008).

The Haimur gold deposit is situated in the western part of the Wadi Allaqi district, where a complexly folded and overturned belt of ophiolites, metavolcanics and metasedimentary rocks are exposed. These rock units form WNW-trending, imbricate sheets, while gold mineralization is confined to tightly-folded, variably carbonatized allochthonous ophiolites embedded in calcareous and locally carbonaceous metasedimentary rocks.

Field work and detailed mapping revealed that the Haimur mine area is underlain by variably silicified and carbonatized serpentinite (listvenite), metagabbro, metabasalt with abundant bands of chert, marble and magnesite. These rocks occur either as mountainous masses or as fragments embedded in pelitic metasediments (mica schist), metasiltstone, metagraywacke and quartz-feldspathic schist. In the mine area, calcareous metasiltstone and mica schist with dolomitic marble bands are common features. Talc and graphite laminae are abundant next to the marble bands. Highly sheared metaandesite, metadacite and pyroclastics, are considered an island arc metavolcanic succession overlain by the ophiolitic rocks (Fig. 1). These rocks have generally metamorphosed under greenschist facies conditions (El-Nisr, 1997). Higher-grade

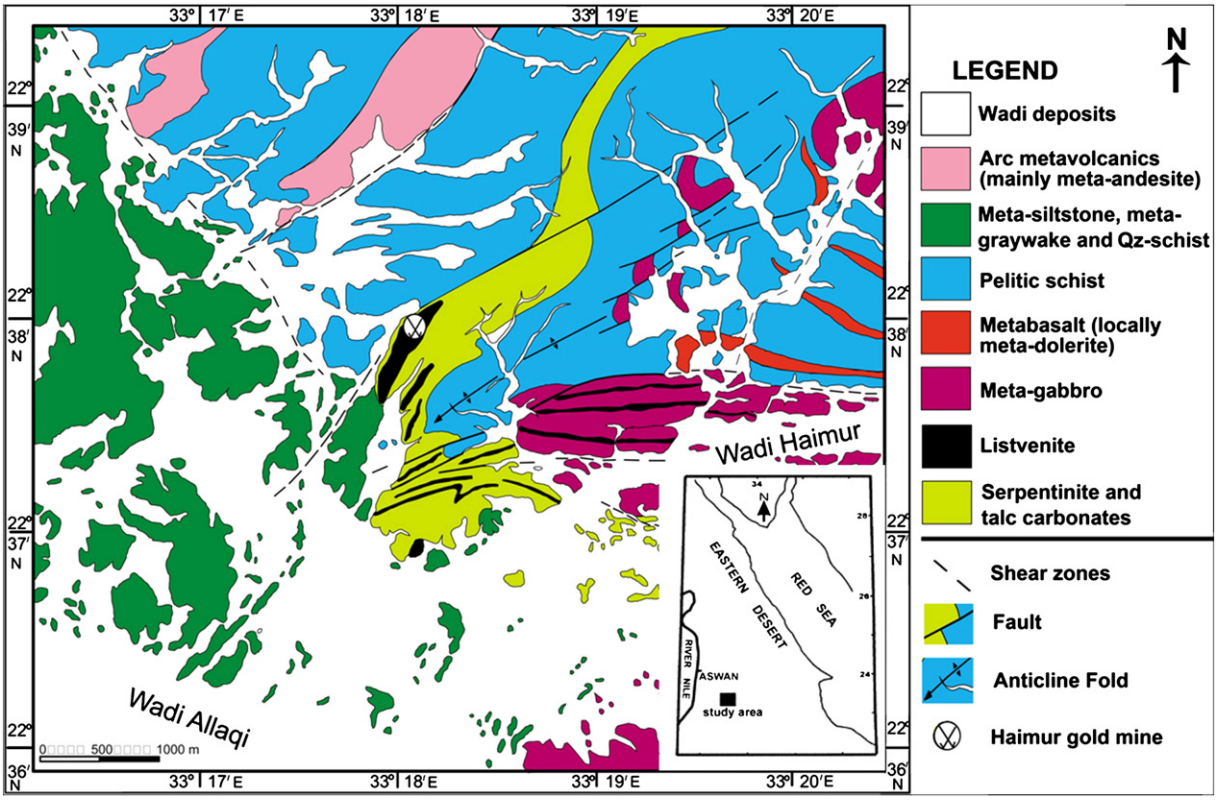

Fig. 1. Geological map of Haimur gold mine area, SE Desert of Eygpt.

Please cite this article as: Emam, A., Zoheir, B., Au and Cr mobilization through metasomatism: Microchemical evidence from ore-bearing listvenite, South Eastern Desert of Egypt, Journal of Geochemical Exploration (2012), http://dx.doi.org/10.1016/j.gexplo.2012.11.004

metamorphism and microstrucutres, amphibolite facies, have been reported in the gneissic and schistose metasediments further north of the mine area and dated as ~600 to 585 Ma (e.g., Abd El-Naby and Frisch, 2002).

The gold mineralization is related to a series of milky and gray quartz lodes associated with highly tectonized, listvenite, along NE-trending, anastomosing shear zones that dip moderately to NW. Based on the discrete kinematic indicators, including stretching lineations and slickenside along the shear zones and on vein walls, the sense of shear is consistently dextral. The mineralized lodes are expressed in irregular and narrow quartz veins, containing subordinate amounts of carbonate and sulfides. These veins extend 25 m or more, and vary from 2 to 100 cm in width. Gold grades in these veins vary from traces up to 35 ppm, and silver is between 0.9 and 15 ppm (Hassaan et al., 1996; Ramadan, 1997; Ramadan et al., 1998, 1999).

4. Mineralogical characteristics

Scanning electron microscope (SEM) investigations of listvenite and listvenzed sepentinite at Haimur mine area revealed that serpentine, dolomite, chlorite, quartz, Cr-spinel and magnetite are the main constituents. Sulfides form euhedral to subhedral crystals as well as fine disseminations incorporated within carbonate and at grain boundaries between the other minerals (Fig. 2A&B). Cr-spinel occurs as euhedral to anhedral disseminated crystals that commonly range from 10 to 500 μm in size (Fig. 2C&D). Under the electron microscope, the details of the metamorphic texture are visible, with bright grains of Cr-spinel occupying interstitial spaces between the dark gray antigorite crystals. The investigated samples show abundant pore spaces that appear as black areas in the BSE images. These voids and crust structures provide clear textural evidence for incipient alteration by percolating fluid and later erosion of less competent materials.

Ore microscopy of the quartz lodes and adjacent altered wallrocks reveal the presence of pyrite, gersdorffite, pyrrhotite, arsenopyrite, pentlandite, subordinate chalcopyrite and rare microscopic gold. The conspicuous feature reported is the association of most disseminated sulfides and sulf-arsenides with slivers of the wallrock incorporated in the mineralized veins. Hydrothermal disseminations include carbonate, chlorite, less common quartz and disseminated sulfides. In the quartz lodes, pyrite occurs as fine disseminations while in listvenite and listvenized serpentinite pyrite forms coarse-grained fresh idiomorphic to xenomorphic crystals with abundant inclusions of gersdorffite, pyrrhotite and chalcopyrite (Fig. 3A&B). Gersdorffite occurs as dispersed euhedral to subhedral crystals, inter-grown with pyrite and pentlandite (Fig. 3C&F). Arsenopyrite is either dispersed as fine disseminations or occurs as inclusions in some pyrite crystals, commonly associated with gersdorffite (Fig. 3E). Chalcopyrite is subordinate in all investigated samples. It occurs commonly as dispersed fine-grained inclusions in pyrite and gersdorffite (Fig. 3A,C,&D). In some cases, inclusions of pyrrhotite are common in the subhedral crystals of pyrite, especially near peripheries. Fine-grained, dispersed subhedral to anhedral pentlandite crystals are associated with pyrite and gersdorffite in the host listvenite (Fig. 3E&F). Gold occurs as fine specks and blebs in quartz veins, commonly associated with dispersed sericite, chlorite and carbonate assemblage. Intergrowth and textural relationships between ore-mineral assemblages of Haimur gold deposit reveal that chalcopyrite, gersdorffite, arsenopyrite, pentlandite and pyrrhotite are early phases, while pyrite and free gold are late in paragenesis.

5. Microchemistry of ore and gangue hydrothermal phases

5.1. Ore minerals

Pyrite is ubiquitous in all investigated samples. It occurs commonly as idiomorphic crystals disseminated in the altered wallrock selvages and quartz lodes. EMPA studies (Table 1) reveal variable contents of As in bright zones (Fig. 4A–C) of the pyrite crystals (up to 2.48 wt.%). Co is absent, while Ni occurs in trace to considerable concentrations (up to 1.49 wt.%). As-bearing cores of large pyrite crystals are associated with inclusions of arsenopyrite, gersdorffite and rare pentlandite (Fig. 4B). The determination of the Pearson's correlation coefficient (r) is the method normally applied for a better understanding of the chemical components of the samples distribution based on geo-statistical studies. Pearson's correlation coefficient values of major and trace elements in

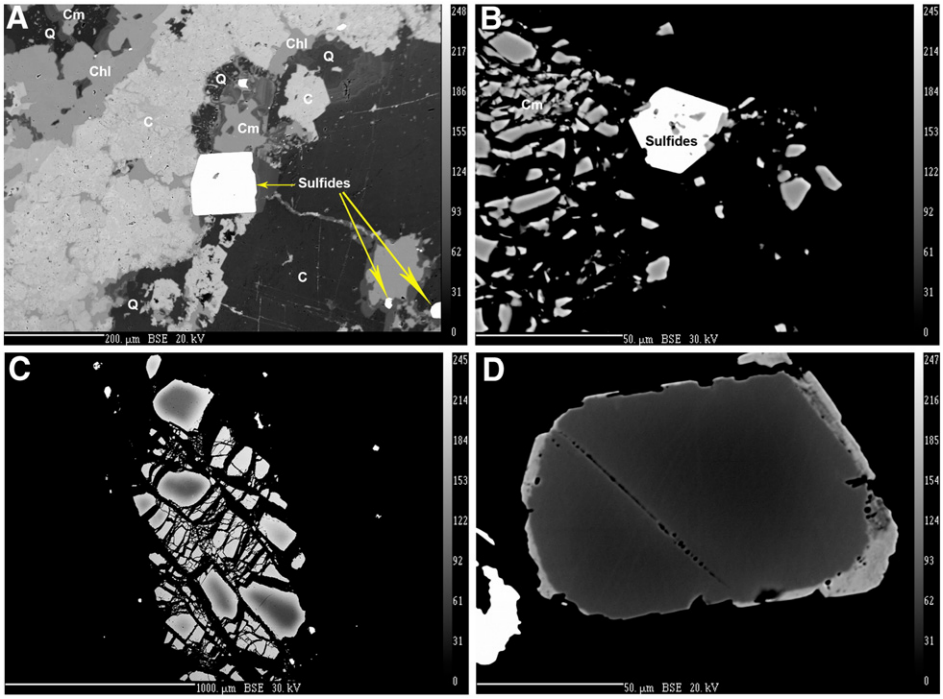

Fig. 2. SEM backscattered electron images of listvenite showing A) carbonates (C), quartz (Q), chlorite (Chl) and Cr-spinel (Cm) as the main mineral constituents, B) euhedral sulfides associated with Cr-spinel (Cm), C) zoned Cr-spinel crystals with dark cores and bright rims, D) Cr-spinel crystal (gray) with ferritchromite rim (light gray).

Please cite this article as: Emam, A., Zoheir, B., Au and Cr mobilization through metasomatism: Microchemical evidence from ore-bearing listvenite, South Eastern Desert of Egypt, Journal of Geochemical Exploration (2012), http://dx.doi.org/10.1016/j.gexplo.2012.11.004

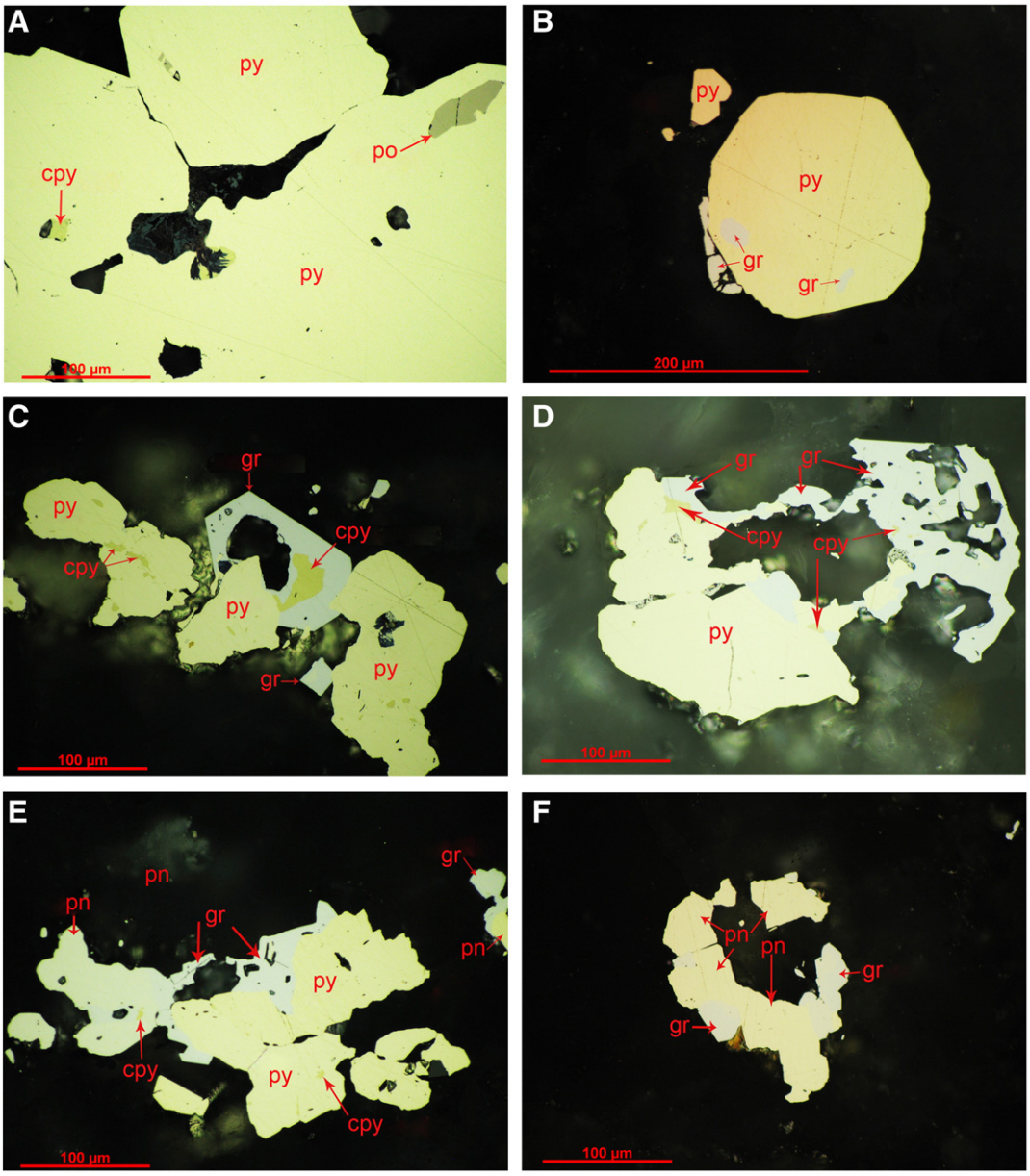

Fig. 3. Microphotographs of ore-minerals; A) coarse-grained pyrite with chalcopyrite and pyrrhotite inclusions, B) idiomorphic pyrite with gersdorffite inclusions, C) euhedral gersdorffite with chalcopyrite inclusions, D) fine pyrite-gersdorffite intergrowth with chalcopyrite inclusions, E) intergrowth of pyrite, gersdorffite, arsenopyrite and pentlandite, F) intergrowth between gersdorffite and pentlandite.

pyrite crystals reveal that gold values are positively correlated with As and Ni, and negatively correlated with Fe and Zn (Table 2).

The chemical composition of arsenopyrite is generally S-rich and depleted in As ($Fe_{1-1.03}As_{0.85-0.96}S_{1.02-1.12}$). Despite the traces of Au (1100–2200 ppm), other trace elements are either absent or straddle the detection limit (Table 3). The correlation coefficient values of major and trace elements in the analyzed arsenopyrite crystals reveal that the Au contents correlate positively with Ni and As values and correlate negatively with Fe and Zn values (Table 4). The structural formula of the analyzed arsenopyrite crystals contain a range of 28.41–32.08 at.% As, which corresponds to formation temperatures of ~300 to 450 °C (Kretschmar and Scott, 1976). Arsenopyrite containing high Au values and associated with gold inclusions has consistently more than 31 at.% As. Substitution of Fe by Au in arsenopyrite is suggested by many authors (e.g., Wu and Delbove, 1989), which may lead to a positive correlation between Au and As. Fleet and Mumin (1997) suggested that invisible Au in arsenopyrite was removed from ore fluids by chemisorption at As-rich, Fe-deficient surface sites and incorporated as a metastable solid-solution. Association of Au and high As zones in arsenopyrite may also suggest deposition of Au in relatively high temperature conditions.

Gersdorffite occurs either in association with pyrite, arsenopyrite and pentlandite, or dispersed in the quartz veins and mineralized wallrock selvages (Fig. 4C&D). Gersdorffite has the ideal composition NiAsS, but significant amounts of iron and cobalt can substitute for nickel, minor amounts of antimony can substitute for arsenic, and sulfur and arsenic may be mutually diadochic (e.g., Balyiss, 1982). In addition to 42.87–44.47 wt.% As and 24.78–34.15 wt.% Ni, the composition of gresdorffite crystals comprises 0.54–9.91 wt.% Fe, up to 4.03 wt.% Co, up to 2.20 wt.% Sb and 0.10–0.20 wt.% Au (Table 5). Single grains of gersdorffite are commonly homogeneous, but inter-elemental ratios (e.g., Ni/Fe, Co/Ni and Co/Fe) are highly variable between grains. Interestingly, the idiomorphic gersdorffite crystals have ideal composition ($Ni_{0.71-0.99}As_{0.96-0.99}S_{0.96-0.099}$) and concentrations of Co, Fe

Please cite this article as: Emam, A., Zoheir, B., Au and Cr mobilization through metasomatism: Microchemical evidence from ore-bearing listvenite, South Eastern Desert of Egypt, Journal of Geochemical Exploration (2012), http://dx.doi.org/10.1016/j.gexplo.2012.11.004

Table 1
Representative EMPA data of pyrite disseminated in quartz veins from Haimur gold mine.

wt.%	1	2	3	4	5	6	7	8	9	10	11	12	13
Fe	47.18	47.29	47.09	46.69	46.65	45.40	45.20	45.88	46.25	46.45	46.69	46.64	46.91
S	52.13	51.97	52.35	52.43	52.17	50.75	50.52	51.30	51.64	51.69	52.00	51.48	51.92
As	0.00	0.00	0.04	0.04	0.00	2.48	2.32	1.32	0.77	0.58	0.23	0.45	0.15
Co	0.00	0.00	0.00	0.00	0.00	0.00	0.00	0.00	0.00	0.00	0.00	0.00	0.00
Ni	0.15	0.25	0.03	0.58	0.19	1.12	1.49	1.05	0.63	0.65	0.32	0.10	0.07
Cu	0.06	0.00	0.00	0.01	0.00	0.00	0.00	0.00	0.00	0.00	0.00	0.00	0.00
Zn	0.02	0.01	0.02	0.00	0.00	0.01	0.00	0.01	0.01	0.01	0.01	0.01	0.01
Ag	0.02	0.02	0.04	0.00	0.03	0.01	0.04	0.02	0.02	0.02	0.02	0.03	0.02
Te	0.00	0.00	0.00	0.00	0.00	0.00	0.00	0.00	0.00	0.00	0.00	0.00	0.00
Au	0.00	0.00	0.01	0.00	0.02	0.04	0.03	0.02	0.02	0.00	0.00	0.00	0.02
Sb	0.00	0.00	0.00	0.00	0.00	0.00	0.00	0.00	0.00	0.00	0.00	0.00	0.00
Sum	99.56	99.54	99.58	99.75	99.06	99.81	99.60	99.60	99.34	99.40	99.27	98.71	99.10
Calculated formula ($Fe_{0.99-1.03}S_{1.94-1.98}$)													
Fe	1.02	1.03	1.02	1.01	1.02	1.00	0.99	1.00	1.01	1.01	1.02	1.02	1.02
S	1.97	1.97	1.98	1.98	1.98	1.94	1.94	1.95	1.96	1.96	1.97	1.97	1.97

and Sb are very low or insignificant. The large irregular grains show heterogenous composition, but not zoned. In terms of atomic% Ni-Fe-Co in the system NiAsS-FeAsS-CoAsS (Klemm, 1965), composition of gersdorffite from the Haimur gold deposit suggests formation temperatures around 400 °C. The calculated Pearson's correlation coefficients of all measured elements are generally low, and slight correlations have been determined between Au, As, Co and Ni (see Table 6).

Pentlandite from Haimur gold deposit is an unusually nickel-rich, Fe-poor variety with a Ni:Fe atomic percent ratio of at least 4 times rather than the normal 1:1 ratio (Table 7). These values are generally higher than those of pentlandite that co-exists with a Ni-Fe phase such as awaruite (Ni_3Fe), but are comparable pentlandite analyses when the coexisting sulfide is a Ni-S phase such as millerite (NiS) or heazlewoodite (Ni_3S_2). Sulfur contents of the analyzed pentlandite (~50 to 55.5 at.%) are greater than the stoichiometric amount of 47.06 atomic %, and consequently the M/S ratio is also higher than the ideal pentlandite composition of M_9S_8. This reflects the real non-stoichiometric composition of the pentlandite, presumably because it replaces the sulfur-rich phases. Analysis of a fine-grained (~3 μm-across) inclusion in zoned pyrite (Fig. 4B) indicates that pyrrhotite is Ni-bearing, and contains several hundreds of ppms of Au. However, scarcity of such inclusions and their small size did not allow more detailed studies on pyrrhotite. Chalcopyrite has consistently a nearly stoichiometric composition ($Cu_{0.96}Fe_{1.07}S_{1.95}$), and contains low concentrations of Ni, 0.38–0.43 wt.% (Table 7).

5.2. Gangue minerals

5.2.1. Cr-spinel

Composition of disseminated chrome spinel crystals has been determined using the electron microprobe technique, under conditions including accelerating voltage of 15 kV, and a beam current of 20 nA (Table 8). The analyzed chrome spinel crystals have generally Cr-rich

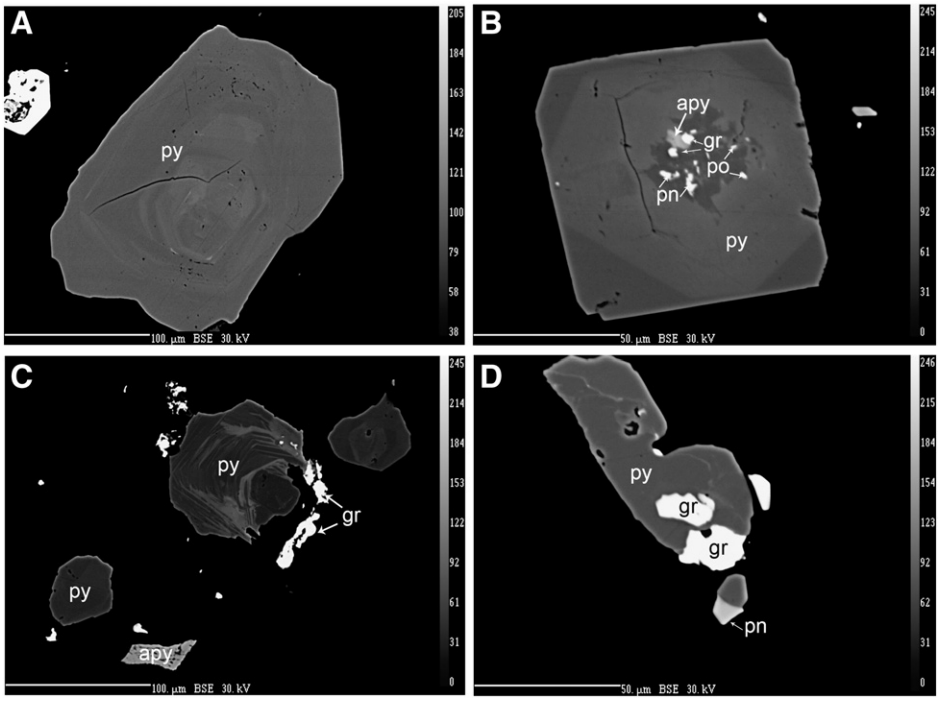

Fig. 4. SEM backscattered electron images showing A) internal zoning in pyrite, B) bright As-bearing core in large pyrite with minute inclusions of gersdorffite, arsenopyrite, pyrrhotite and pentlandite, C) zoned pyrite and fine gersdorffite disseminations, D) gersdorffite-pyrite intergrowth.

Please cite this article as: Emam, A., Zoheir, B., Au and Cr mobilization through metasomatism: Microchemical evidence from ore-bearing listvenite, South Eastern Desert of Egypt, Journal of Geochemical Exploration (2012), http://dx.doi.org/10.1016/j.gexplo.2012.11.004

Table 2
Spearman rank-correlation coefficients (r) at the 95% confidence level calculated to evaluate correlations between major and trace elements in pyrites. Calculations are based on the 7 analyses in Table 1, in which gold triggers the detection limit.

	Fe	S	As	Ni	Zn	Ag
S	**0.924**					
As	**−0.960**	**−0.957**				
Ni	**−0.937**	**−0.893**	**0.926**			
Zn	0.456	0.413	−0.312	−0.417		
Ag	0.072	0.103	−0.130	−0.102	−0.108	
Au	**−0.744**	**−0.625**	**0.750**	0.632	−0.345	−0.100

Values in bold are those considered significant.

Table 4
Pearson's correlation coefficients (r) calculated to investigate the interrelationship between major and trace elements in pyrites. Calculations are based on data in Table 3.

	Fe	S	As	Ni	Cu	Zn	Ag	Au
S	**0.735**							
As	**−0.671**	**−0.986**						
Ni	**−0.892**	**−0.511**	**0.452**					
Cu	**−0.408**	−0.198	0.152	0.378				
Zn	−0.085	−0.229	0.209	0.154	**−0.542**			
Ag	−0.277	−0.169	0.053	0.197	**0.597**	−0.204		
Au	**−0.413**	−0.251	0.215	**0.532**	−0.129	0.128	−0.029	

Values in bold are those considered significant.

cores and Fe-rich rim. MnO is generally absent in all of the analyzed crystals. V_2O_5 contents vary from 0.17 to 0.35 wt.%. Traces of TiO_2 (up to 0.77 wt.%) have been determined in the Al-rich, Cr-spinel crystals. Erratic MgO content in the Cr-spinel and chromite crystals can be attributed to beam hits in the vicinity of discrete, very minute inclusion of chlorite in the analyzed crystals.

Although generally insignificant, SiO_2 (up to 0.16 wt.%) has been only detected at crystal boundaries, which may suggest possible contamination from the silicate matrix. The Al_2O_3 contents vary from 4.78 to 11.86 in the analyzed crystals, with notable increase in cores of the Cr-spinel crystals. Slivers of the wallrock material in the mineralized quartz veins commonly contain Cr-spinel crystals and chlorite, commonly intergrown with sericite and hydrothermal quartz. The analyzed Cr-spinel grains are generally characterized by high chromite component with a Cr# [Cr/(Cr + Al)] of 0.89, and variable Fe# [Fe/(Fe + Mg)] values (0.57–0.97). In contrast, a large crystal of Cr-spinel in the wallrock slivers within quartz veins have Fe# values of 0.85–0.98 and Cr# values of 0.75 to 0.86. In many grains, the Cr# is identical and the compositional zoning is almost entirely due to an increase in Fe^{II}/(Fe^{II} + Mg) value towards the rim (see Table 8). These zoned crystals show typical enrichment in Fe^{II} and Fe^{III} in the rim and gradual depletion in Cr, Al and Mg from core to rim.

Generally, the analyzed spinel gains pertain to Al-chromite. The high Cr#, low TiO_2 contents, coupled with variable but generally low Al_2O_3 contents suggest a supra-subduction zone, back-arc tectonic setting for the host serpentinite (e.g., Barnes and Roeder, 2001). Highly variable ferrous/ferric iron ratios (4–37) may indicate variable oxidation during low grade metamorphism, or significant hydrothermal alteration. The association of chromite with Cr-spinel and Cr-chlorite is suggested to be the result of the common metasomatic alteration of chromitites and formation of a ferritchromite + Cr-chlorite assemblage, partially replacing chromite + serpentine assemblages (e.g., Barnes, 2000; Mellini et al., 2005).

$$\underset{\text{(chromite/Cr−spinel)}}{2(Mg,Fe)(Cr,Al)_2O_4} + \underset{\text{(Antigorite)}}{1.5(Mg,Al,Fe)_3Si_2O_5(OH)_4} + H_2O + 0.15O_2 \rightarrow$$
$$\underset{\text{(ferrichromite)}}{1.2(Mg,Fe)(Cr,Fe,Al)_2O_4} + \underset{\text{(Cr−chlorite)}}{0.5(Mg,Fe,Al,Cr)_{12}(Al_2Si_6)O_{20}(OH)_{16}}$$

Cr-spinel grains that have relatively Mg-Cr rich cores are rimed by more Fe-rich composition formulated as $(Mg_{0.15}, Fe_{0.85})(Cr_{1.71}, Al_{0.22}, Fe_{0.07})O_4$. Some grains have cores with similar composition to these rims, but overgrown by ferrichromite $(Mg_{0.01}, Fe_{0.99})(Cr_{1.61}, Al_{0.07}, Fe_{0.23})O_4$. It is suggested that Fe-bearing rims in less oxidized grains were products of exchange of Fe^{2+} from olivine and Mg from chromite/Cr-spinel during serpentinization of the original ultramafic rocks. On the other hand, ferrichromite rims have developed due to interaction of chromite/Cr-spinel with serpentine minerals during listvenization of serpentinites.

5.2.2. Fuchsite and Cr-chlorite

Green muscovite flakes are disseminated in the altered wallrocks next to quartz veins and in selvages of the host rock in the mineralized lodes. A petrographic relationship has been established between these mica flakes and chromite/Cr-spinel and serpentine, dolomite and chlorite (see Fig. 2A). The green color could be the result of Cr substitution in this mica type (fuchsite; $K(Al,Cr)_2[(OH,F)_2/AlSi_3O_{10}]$). The Cr_2O_3 values measured in some flakes (up to 1.94 wt.%) along with the intimate association with chromite suggest formation through metasomatic alteration of originally Cr-spinels. However, the high silica content (48.48–50.46 wt.%) and low FeO values (up to 0.77 wt.%) may indicate partial metasomatism 'listvenitization' or limited fluid flux. Compositional

Table 3
Representative EMPA data of arsenopyrite from Haimur gold deposit.

wt.%	1	2	3	4	5	6	7	8	9	10
Fe	35.82	36.57	36.31	35.82	34.32	35.21	36.38	34.19	36.62	36.53
S	20.36	22.23	21.57	21.14	21.33	21.35	22.33	20.10	22.60	22.75
As	44.04	41.61	42.40	42.71	42.43	42.65	40.86	43.96	40.94	40.59
Co	0.00	0.00	0.00	0.00	0.00	0.00	0.00	0.00	0.00	0.00
Ni	0.01	0.00	0.00	0.00	0.05	0.01	0.00	0.04	0.01	0.00
Cu	0.00	0.00	0.00	0.01	0.01	0.00	0.00	0.00	0.00	0.00
Zn	0.02	0.00	0.00	0.00	0.00	0.01	0.01	0.02	0.02	0.01
Ag	0.01	0.01	0.00	0.03	0.02	0.00	0.02	0.02	0.00	0.02
Te	0.03	0.02	0.00	0.06	0.03	0.00	0.01	0.05	0.00	0.00
Au	0.20	0.15	0.19	0.11	0.22	0.16	0.19	0.19	0.14	0.18
Sb	0.00	0.05	0.00	0.02	0.00	0.00	0.11	0.00	0.00	0.01
Total	100.49	100.64	100.47	99.9	98.41	99.39	99.92	98.58	100.33	100.08
Calculated formula ($Fe_{1.0–1.3}As_{0.85–0.96}S_{1.02–1.12}$)										
Fe	1.03	1.03	1.03	1.03	1.00	1.01	1.03	1.00	1.03	1.03
S	1.02	1.09	1.07	1.06	1.08	1.07	1.10	1.03	1.11	1.12
As	0.94	0.87	0.90	0.91	0.92	0.91	0.86	0.96	0.86	0.85
Total	3	3	3	3	3	3	3	3	3	3

Please cite this article as: Emam, A., Zoheir, B., Au and Cr mobilization through metasomatism: Microchemical evidence from ore-bearing listvenite, South Eastern Desert of Egypt, Journal of Geochemical Exploration (2012), http://dx.doi.org/10.1016/j.gexplo.2012.11.004

Table 5
Representative EMPA data of gersdorffite disseminated in quartz lodes from Haimur gold deposit.

wt.%	1	2	3	5	6	7	10	11	12	13	14	15	16	17	18	19	20	21	22	23	24	25	26	27
Fe	8.75	9.36	9.08	1.37	9.43	9.11	4.33	8.39	7.69	9.91	2.41	1.88	1.4	1.24	1.32	4.9	5.43	1.22	1.79	1.34	0.91	0.83	0.85	0.54
S	18.72	18.93	18.69	18.18	18.95	18.77	18.95	18.54	18.69	18.87	18.56	18.62	18.73	18.74	18.12	19.1	19.24	18.64	18.58	18.46	18.43	18.41	18.72	18.56
As	44.39	43.98	44.2	43.41	43.84	44.28	43.42	44.47	44.33	43.96	43.83	43.3	43.32	42.87	43.34	43.29	43.64	43.89	43.37	43.5	43.12	43.28	43.94	43.23
Co	0	0.75	0.86	0.12	0.9	1.53	0.18	1.25	0.56	0.78	1.22	1.79	1.35	1.18	1	3.41	4.03	0.6	0.69	1.34	1.35	0.86	1.9	1.14
Ni	26.94	25.69	25.6	33.49	25	24.79	32.84	25.73	27.35	24.78	32.8	31.8	32.83	33.7	33.23	28.04	26.56	33.45	33.3	33.22	33.71	34.15	32.48	33.78
Cu	0	0	0	0	0	0	0	0	0	0	0	0	0	0	0	0	0	0	0	0	0	0	0	0
Zn	0.03	0.01	0	0.02	0.01	0.03	0.02	0.01	0.02	0.04	0	0.02	0.02	0.02	0.02	0.01	0.01	0.03	0.02	0.03	0.01	0.02	0.01	0.01
Ag	0.01	0.02	0	0.01	0.01	0.01	0	0	0	0	0	0.01	0.01	0	0.02	0.02	0	0	0	0	0.01	0	0.01	0
Te	0	0	0	0	0	0	0	0	0	0	0	0	0	0	0	0	0	0	0	0	0	0	0	0
Au	0.12	0.13	0.14	0.13	0.14	0.14	0.1	0.13	0.15	0.16	0.13	0.14	0.19	0.18	0.14	0.17	0.15	0.15	0.14	0.2	0.15	0.18	0.16	0.19
Sb	0.07	0.06	0	2.2	0.01	0.04	0.45	0.03	0.07	0.03	0.12	0.56	0.7	0.73	1.55	0.39	0.15	0.7	0.54	0.87	0.89	0.84	0.75	0.88
Sum	99.03	98.93	98.57	98.93	98.29	98.7	100.29	98.55	98.86	98.53	99.07	98.12	98.55	98.66	98.74	99.33	99.21	98.68	98.43	98.96	98.58	98.57	98.82	98.33
Ratios																								
Co/Ni	0	0.03	0.03	0	0.04	0.06	0.01	0.05	0.02	0.03	0.04	0.06	0.04	0.04	0.03	0.12	0.15	0.02	0.02	0.04	0.04	0.03	0.06	0.03
Ni/Fe	3.08	2.74	2.82	24.45	2.65	2.72	7.58	3.07	3.56	2.5	13.61	16.91	23.45	27.18	25.17	5.72	4.89	27.42	18.6	24.79	37.04	41.14	38.21	62.56
Co/Fe	0	0.08	0.09	0.09	0.1	0.17	0.04	0.15	0.07	0.08	0.51	0.95	0.96	0.95	0.76	0.7	0.74	0.49	0.39	1	1.48	1.04	2.24	2.11
Formula	$(Fe_{0.02-0.30}Ni_{0.71-0.99}As_{0.96-1.00}S_{0.96-1.00})$																							
S	0.98	0.99	0.98	0.97	0.99	0.98	0.98	0.97	0.98	0.99	0.97	0.98	0.99	0.99	0.96	0.99	1	0.98	0.98	0.97	0.97	0.97	0.99	0.98
As	0.99	0.98	0.99	0.99	0.98	0.99	0.96	1	0.99	0.98	0.98	0.98	0.98	0.96	0.98	0.96	0.97	0.99	0.98	0.98	0.97	0.98	0.99	0.98
Ni	0.77	0.73	0.73	0.97	0.71	0.71	0.92	0.74	0.78	0.71	0.94	0.92	0.94	0.97	0.96	0.8	0.75	0.96	0.96	0.95	0.97	0.99	0.93	0.98

Table 6
Pearson's correlation coefficient values of major and trace elements in gersdorffite from Haimur gold deposit.

	Fe	As	Co	Ni	Zn	Ag	Au
As	**0.767**						
Co	−0.044	−0.108					
Ni	**−0.970**	**−0.757**	−0.165				
Zn	−0.193	−0.202	−0.180	0.225			
Ag	0.032	−0.105	**0.244**	−0.100	−0.103		
Au	**−0.405**	**−0.359**	**0.332**	**0.302**	0.267	−0.037	
Sb	**−0.753**	**−0.622**	−0.177	**0.746**	0.274	0.232	0.211

Values in bold are those considered significant.

variations observed in the Cr, Fe and Mg contents in fuchsite and Cr-rich chlorite (Table 9) could be explained by an original heterogeneous distribution of these elements in the igneous spinels.

Near stoichiometric, Cr-bearing chlorite ($Mg_{3.95-3.71}Fe^{II}_{0.98-0.72}Cr_{0.27-0.20}Si_{3.08-2.87}Al_{2.24-1.94}O_{10}(OH)_8$ is associated with fuchsite and relict Cr-spinel. EMPA analyses of Cr-chlorite indicate homogenous compositional range, where TiO_2, MnO, CaO, Na_2O, K_2O and BaO are mostly absent while Mg# (0.84–0.80) and MgO content (24.43 to 26.12 wt.%) are nearly identical. Also, FeO concentrations vary from 8.69 to 11.06 wt.%, and traces of V_2O_5 and SrO have been determined in most of the analyzed flakes (see Table 9). Calculated on basis of the empirical chlorite geothermometer equation of Kranidiotis and MacLean (1987), which gives better results for highly magnesian chlorites (e.g., Frimmel, 1997), a temperature range of 238 to 268 °C is estimated as the formation temperatures of the analyzed chlorites.

5.2.3. Carbonate minerals

Carbonate minerals are intergrown with hydrothermal quartz and form veinlets and network in the wallrock slivers enclosed in the quartz veins. Carbonate minerals occur also as coarse patches in quartz lodes and as fine aggregated disseminations associated with sulfides. The EPMA data indicate a nearly homogenous dolomite or ferroan dolomite composition (Table 10). The MnO and SrO proportions are consistently low, and the BaO content is low or even nonexistent. Although most analyzed samples show comparable composition of carbonate, variable Fe# (0.09–0.41) and Mg# (0.53–0.91) suggest variable solubility of these elements in the metasomatic system. The dolomite component ($CaMg(CO_3)_2$) varies from 51 to 84 mol%. The ankerite component ($CaFe(CO_3)_2$) comes next with a range of 7.28 to 34.73 mol%. Kutnohorite ($CaMn(CO_3)_2$) form up to ~10 mol%. Strontianite ($SrCO_3$) occurs as high as ~4 mol%. The other components are either absent or insignificant, forming less than 1 mol%. Homogeneity in the composition of

Table 7
Representative EMPA data of pentlandite and chalcopyrite from Haimur gold deposit.

wt.%	Pentlandite					Chalcopyrite		
Fe	11.34	11.35	3.72	5.40	6.60	Fe	31.83	32.22
S	35.82	35.25	39.95	39.77	38.89	S	33.40	33.87
As	0.00	0.00	0.00	0.04	0.01	As	0.03	0.05
Co	0.00	0.15	0.01	0.03	0.05	Co	0.00	0.04
Ni	52.59	52.25	55.78	52.51	53.21	Ni	0.38	0.43
Cu	0.00	0.02	0.00	1.21	1.14	Cu	32.61	33.10
Zn	0.03	0.01	0.02	0.04	0.06	Zn	0.03	0.00
Ag	0.02	0.01	0.01	0.00	0.00	Ag	0.06	0.00
Te	0.00	0.00	0.00	0.00	0.00	Te	0.00	0.00
Au	0.00	0.00	0.00	0.00	0.00	Au	0.00	0.00
Sum	99.80	99.04	99.49	99.00	99.96	Sum	98.34	99.71
Formula	$(Fe_{0.5-1.57},Ni_{6.83-7.14})_9S_8$					Formula	$Cu_{0.96}Fe_{1.07}S_{1.95}$	
Fe	1.56	1.57	0.50	0.73	0.89	Fe	1.07	1.07
S	8.57	8.51	9.36	9.36	9.14	S	1.95	1.95
Ni	6.87	6.89	7.14	6.75	6.83	Cu	0.96	0.96

Table 8
Representative electron microprobe data of Cr-spinel grains associated with slivers of wallrock in the mineralized quartz veins.

	Cr-spinel fresh grains										Single Cr-spinel grain with a ferritchromite rim									
wt.%	Rim	Rim	Core	Core	Rim	Rim	Core	Rim	Rim	Core	Rim	Rim			Core					Rim
SiO_2	0.02	0.01	0.02	0.02	0.01	0.04	0.02	0.03	0.02	0.03	0.02	0.16	0.04	0.04	0.03	0.02	0.03	0.03	0.02	0.13
TiO_2	0.00	0.02	0.02	0.05	0.00	0.05	0.02	0.06	0.04	0.00	0.03	0.03	0.01	0.03	0.77	0.13	0.10	0.05	0.14	0.41
Al_2O_3	4.78	5.02	5.21	5.27	5.25	5.09	4.85	5.24	4.91	5.01	5.19	4.96	5.26	5.01	5.56	10.09	9.61	11.86	10.70	8.61
Cr_2O_3	58.61	60.05	62.70	63.18	62.91	60.33	59.86	62.50	59.33	60.04	62.80	59.99	62.84	59.70	50.01	51.92	55.91	54.08	53.31	50.07
V_2O_3	0.25	0.32	0.20	0.35	0.25	0.18	0.30	0.27	0.21	0.24	0.26	0.33	0.23	0.17	0.18	0.23	0.22	0.31	0.33	0.17
FeO	32.42	29.37	21.30	21.21	21.70	28.67	30.67	22.24	31.50	29.94	21.94	30.17	21.55	30.55	41.03	32.04	31.14	31.07	33.04	39.31
MgO	0.69	3.22	8.65	8.75	8.51	3.69	1.95	8.18	1.60	2.76	8.35	2.67	8.49	2.15	0.38	2.35	3.08	3.04	2.37	2.43	1.51
CaO	0.06	0.02	0.00	0.00	0.00	0.07	0.10	0.01	0.04	0.03	0.00	0.07	0.00	0.01	0.01	0.00	0.01	0.00	0.00	0.00	0.00
ZnO	1.29	0.22	0.11	0.10	0.13	0.27	0.73	0.09	0.64	0.45	0.10	0.47	0.11	0.59	0.41	0.54	0.41	0.49	0.59	0.54	0.50
Total	98.12	98.25	98.21	98.9	98.81	98.34	98.53	98.58	98.31	98.54	98.66	98.72	98.52	98.23	98.51	97.34	100.5	100.9	100.5	100.4	100.7
Structural formula calculated on basis of 4 oxygens																					
Si	0.00	0.00	0.00	0.00	0.00	0.00	0.00	0.00	0.00	0.00	0.00	0.00	0.00	0.00	0.01	0.00	0.00	0.00	0.00	0.00	0.00
Ti	0.00	0.00	0.00	0.00	0.00	0.00	0.00	0.00	0.00	0.00	0.00	0.00	0.00	0.00	0.02	0.00	0.00	0.00	0.00	0.00	0.01
Al	0.21	0.21	0.21	0.21	0.21	0.22	0.21	0.21	0.21	0.21	0.21	0.21	0.21	0.21	0.24	0.42	0.39	0.48	0.44	0.42	0.35
Cr	1.71	1.71	1.72	1.72	1.71	1.71	1.72	1.71	1.71	1.71	1.71	1.71	1.72	1.72	1.44	1.47	1.53	1.46	1.46	1.39	1.38
V	0.01	0.01	0.01	0.01	0.01	0.01	0.01	0.01	0.01	0.01	0.01	0.01	0.01	0.00	0.01	0.01	0.01	0.01	0.01	0.01	0.00
Fe(III)	0.07	0.06	0.06	0.06	0.06	0.07	0.06	0.07	0.07	0.06	0.06	0.07	0.06	0.06	0.26	0.09	0.07	0.05	0.09	0.18	0.23
Fe(II)	0.93	0.82	0.55	0.55	0.56	0.79	0.87	0.58	0.90	0.84	0.57	0.84	0.56	0.87	0.99	0.87	0.83	0.84	0.87	0.86	0.92
Mg	0.04	0.17	0.45	0.45	0.44	0.20	0.11	0.42	0.09	0.15	0.43	0.14	0.44	0.12	0.02	0.13	0.16	0.15	0.12	0.13	0.08
Ca	0.00	0.00	0.00	0.00	0.00	0.00	0.00	0.00	0.00	0.00	0.00	0.00	0.00	0.00	0.00	0.00	0.00	0.00	0.00	0.00	0.00
Zn	0.04	0.01	0.00	0.00	0.00	0.01	0.02	0.00	0.02	0.01	0.00	0.01	0.00	0.02	0.01	0.01	0.01	0.01	0.02	0.01	0.01
Total	3.00	3.00	3.00	3.00	3.00	3.00	3.00	3.00	3.00	3.00	3.00	3.00	3.00	3.00	3.00	3.00	3.00	3.00	3.00	3.00	3.00
Fe/Fe + Mg	0.96	0.84	0.58	0.58	0.59	0.81	0.90	0.60	0.92	0.86	0.60	0.86	0.59	0.89	0.98	0.88	0.85	0.85	0.89	0.89	0.94
Cr/Cr + Al	0.89	0.89	0.89	0.89	0.89	0.89	0.89	0.89	0.89	0.89	0.89	0.89	0.89	0.89	0.86	0.78	0.80	0.75	0.77	0.77	0.80

the analyzed carbonate grains may refer to equilibrium or near close system.

6. Discussion

6.1. Listvenite formation

Listvenite is formed by the development of micro-crystalline and macro-crystalline quartz due to the removal of silica from serpentinites. The introduction of silica and other elements such as Au, Ag, Cu, Pb, Sb, As, Rb, Ba, K in circulating hydrothermal fluids is crucial for listvenite formation (e.g., Akbulut et al., 2006; Uçurum, 2000). Serpentinite is transformed into talc and magnesite at CO_2-content of the fluid >2–6 mol% (under fluid pressure of 2 kbar: Johannes, 1969) and temperature >300 °C (e.g., Hansen et al., 2005; Robinson et al., 2005). When the temperature decreases (<300 °C), serpentinite reacts with the fluids to form magnesite and quartz, according to the following schematic reaction (Boschi et al., 2009):

$$\underset{\text{(serpentine)}}{Mg_3Si_2O_5(OH)_4} + 3\underset{\text{(gas)}}{CO_2} \rightarrow 3\underset{\text{(magnesite)}}{MgCO_3} + 2\underset{\text{(quartz)}}{SiO_2} + 2H_2O$$

In Haimur gold mine area, listvenite zones are exposed as several hundred meters long and ~150 m wide elongate bodies. They are characterized by pale green to yellowish green color in the hand-specimens, whereas the surface samples exhibit reddish brown color due to oxidation of Fe-bearing minerals to iron oxides. It is composed mainly of Fe–Mg carbonate, quartz and Cr-bearing white mica, together with disseminated chromite, Cr-spinel and sulfides. In the Haimur mine, abundant quartz in listvenite zones suggests that listvenitization caused by relatively low pH fluids (sensu stricto Boschi et al., 2009).

The association of disseminated Cr-chlorite and fuchsite with Fe-Mg carbonate in listvenite wallrock and slivers in the mineralized quartz lodes in Haimur deposit suggests Cr mobilization by CO_2-rich hydrothermal fluids (e.g., Pan and Fleet, 1989). Fuchsite formation is attributed to alteration of Cr-rich phases (Cr-spinels) due to a high a_{CO2} (responsible for the formation of the paragenetic carbonates) and K^+-rich hydrothermal fluids. The intergrowth textures of these minerals with hydrothermal quartz suggest that listvenitization was likely concomitant with quartz veining.

6.2. Element mobility and gold mineralization

Gold-bearing listvenites can form by influx of deep-seated, CO_2-rich reduced ore fluids, and subsequent temperature decrease under high redox potential and low pH conditions (Akbulut et al., 2006 and references therein). Decrease of solubility of gold and other metals and their precipitation are caused primarily by mixing of CO_2-free endogenous solutions with CO_2-rich surface waters (e.g., Pal'yanova and Kolonin, 2004). By contrast, solutions of increasing alkalinity increase the mobility of Au at the expense of hydrosulfides, resulting in its partial removal from listvenite at the corresponding stages of ore formation. Thus, the influence of pH is crucial in the gold potential of listvenites and processes of their mineralization (Likhoidov et al., 2007). The presence of carbonate minerals makes listvenites favorable for the precipitation of Au in systems with repeated influx of ore-bearing fluids.

The experimental work by Likhoidov et al. (2007) showed that the interaction of serpentinite with "pure" water produces a weakly alkaline environment and low gold solubility. The addition of CO_2 to the aqueous solution leads to further decrease of the bulk solubility of Au. The bulk solubility of Au in a 1 mol KCl solution environment increases even in the presence of CO_2 owing to the appearance of its chloride species. According to Kolonin et al. (1997), addition of CO_2 to the serpentinite-water system decreases the bulk solubility of Au, particularly in the KCl environment owing to salting out. The bulk solubility of Au is governed by the redox potential as well. Changes in

Please cite this article as: Emam, A., Zoheir, B., Au and Cr mobilization through metasomatism: Microchemical evidence from ore-bearing listvenite, South Eastern Desert of Egypt, Journal of Geochemical Exploration (2012), http://dx.doi.org/10.1016/j.gexplo.2012.11.004

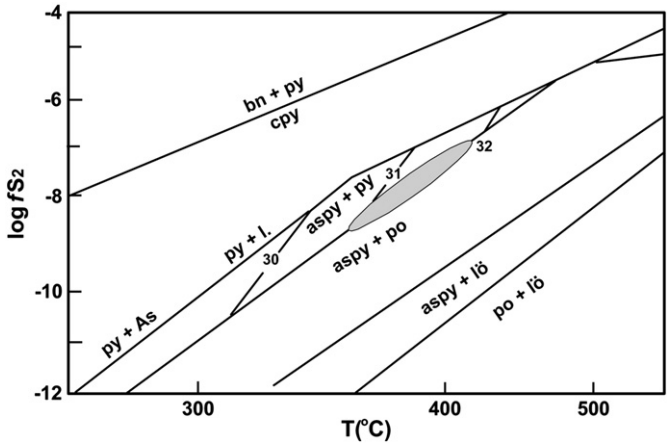

Fig. 5. Activity of S_2 temperature projection of the stability field of arsenopyrite (Barton, 1969), with atomic wt.% As arsenopyrite buffered curves from Kretschmar and Scott (1976). The hatched area depicts temperatures of around 400 °C and log fS_2 around −8 as conditions of precipitation auriferous arsenopyrite in the Haimur gold deposit. As, arsenic, aspy, arsenopyrite, bn, bornite, l, liquid, lö, loellingite, po, pyrrhotite, py, pyrite.

fO_2 into reducing environment always foster Au concentration in the fluid (Likhoidov et al., 2007).

Gold is transported via sulfide–arsenide complexes in the CO_2-H_2O-rich hydrothermal solutions (e.g. Buisson and Leblanc, 1987; Leblanc and Fischer, 1990) and precipitated during the introduction of silica (Buisson and Leblanc, 1987). Buisson and Leblanc (1987) indicated that gold is associated with cobalt–arsenide mineralization in Bou Azzer (Morocco) ophiolite complex, whereas in the serpentinite massifs of the Arabian shield, it is associated with the pyrite-rich portions of gersdorffite (NiAsS)-bearing listvenite lenses and late-stage 'en-echelon' quartz veins. Auclair et al. (1993) noted that alteration zones in the Eastern Metals Ni-Cu-Zn Deposit are rich in Cr, Ni and Co. Consequently, the low temperature alteration assemblages in the ophiolitic terrains would show positive correlations between Ni, Au, As and Co.

The Ni-As-Fe sulfide-bearing listvenite at Haimur mine are examples of talc-carbonate alteration assumed to have been concomitant with sulfidation in response to infiltration of a fluid with sufficient CO_2 to form significant amounts of carbonate (sensu Groves and Keays, 1979). The euhedral habit of several gersdorffite crystals, and the association of arsenopyrite, pentlandite and pyrrhotite, commonly as inclusions in pyrite, may indicate formation at relatively higher temperatures (~400 °C). Pyrrhotite is replaced by pyrite with up to 1 at.% Ni. The dispersed anhedral gersdorffite implies the introduction of arsenic (in particular) through mobilization by CO_2-rich fluids during greenschist facies metamorphism/deformation of the host rocks and by hydrothermal fluids (probably from un-exposed granitoids) that also carried nickel and cobalt scavenged from the ultramafic rock. The positive correlation between Ni and As in the disseminated pyrite and arsenopyrite argues for the dissolution of Ni-bearing phases of serpentinite during carbonatization. The liberated Ni was then re-precipitated as nickel–arsenide complexes due to the increasing sulfur and oxygen fugacities during silicification.

6.3. Temperature, fO_2 and fS_2 conditions of the metasomatism/mineralization

The oxygen and sulfur fugacity (fO_2 and fS_2) are considered critical in formation of sulfide phases during serpentinization and following metasomatism (e.g., Auclair et al., 1993; Frost, 1985; Groves and Keays, 1979). Infiltration of a CO_2-rich fluid into peridotite at temperatures below 400 °C can produce a significant amount of carbonate

Table 9
Representative electron microprobe data of fuchsite and Cr-chlorite disseminated in the mineralized lodes.

	Fuchsite						Chlorite						
SiO_2	49.13	50.06	50.46	49.66	48.48		28.29	29.45	28.56	30.93	29.95	28.13	28.29
TiO_2	0.29	0.25	0.03	0.05	0.05		0.04	0.02	0.05	0.00	0.02	0.02	0.04
Al_2O_3	32.05	32.79	33.43	34.13	34.76		18.48	16.74	17.70	18.06	17.16	18.29	18.48
FeO	0.77	0.66	0.28	0.20	0.19		9.24	9.50	9.68	8.69	9.28	9.21	9.24
MnO	0.03	0.04	0.04	0.05	0.03		0.00	0.00	0.00	0.00	0.00	0.00	0.00
MgO	1.56	1.56	0.88	0.39	0.30		24.43	26.06	26.12	25.03	25.72	25.61	24.43
CaO	0.24	0.17	0.10	0.09	0.13		0.00	0.04	0.04	0.06	0.05	0.05	0.00
BaO	0.00	0.00	0.00	0.00	0.00		0.00	0.00	0.01	0.00	0.00	0.00	0.00
SrO	0.00	0.00	0.00	0.00	0.00		0.18	0.16	0.21	0.11	0.17	0.16	0.18
V_2O_3	0.00	0.00	0.00	0.00	0.00		0.10	0.06	0.11	0.08	0.08	0.09	0.10
Cr2O3	1.94	0.87	0.89	0.73	0.75		5.74	5.06	5.23	5.01	6.10	5.44	5.74
Na_2O	0.24	0.26	0.97	1.42	0.88		0.01	0.00	0.04	0.01	0.04	0.02	0.01
K_2O	6.93	6.18	6.05	6.43	7.71		0.04	0.02	0.02	0.03	0.02	0.02	0.04
Total	93.16	92.82	93.12	93.13	93.26		86.55	87.11	87.78	88.01	88.59	87.04	85.81
Formula based on 11 anions							Formula based on 14 anions						
T2	4.03	3.98	3.96	3.97	4.00		6.18	6.11	6.09	5.98	6.04	6.13	6.37
Si	3.92	4.00	4.03	3.97	3.87		2.91	2.99	2.89	3.08	3.01	2.87	2.97
Ti	0.02	0.02	0.00	0.00	0.00		0.00	0.00	0.00	0.00	0.00	0.00	0.00
Al	3.02	3.09	3.15	3.21	3.27		2.24	2.01	2.11	2.12	2.03	2.20	1.94
Fe(II)	0.05	0.04	0.02	0.01	0.01		0.79	0.81	0.82	0.72	0.78	0.79	0.98
Mn	0.00	0.00	0.00	0.00	0.00		0.00	0.00	0.00	0.00	0.00	0.00	0.00
Mg	0.19	0.19	0.10	0.05	0.04		3.74	3.95	3.95	3.71	3.85	3.90	3.86
Ca	0.02	0.01	0.01	0.01	0.01		0.00	0.00	0.00	0.01	0.01	0.01	0.01
Ba	0.00	0.00	0.00	0.00	0.00		0.00	0.00	0.00	0.00	0.00	0.00	0.00
Sr	0.00	0.00	0.00	0.00	0.00		0.03	0.03	0.04	0.02	0.03	0.03	0.03
V	0.00	0.00	0.00	0.00	0.00		0.01	0.01	0.01	0.01	0.01	0.01	0.01
Cr	0.06	0.03	0.03	0.02	0.02		0.23	0.20	0.21	0.20	0.24	0.22	0.27
Na	0.04	0.04	0.15	0.22	0.14		0.00	0.00	0.01	0.00	0.01	0.00	0.00
K	0.71	0.63	0.62	0.66	0.79		0.01	0.00	0.00	0.00	0.00	0.00	0.00
Total	8.02	8.04	8.11	8.15	8.15		9.97	10.00	10.05	9.87	9.98	10.03	10.07
X_{Ms}	0.95	0.94	0.80	0.75	0.85	Mg#	0.82	0.83	0.83	0.84	0.83	0.83	0.80

Please cite this article as: Emam, A., Zoheir, B., Au and Cr mobilization through metasomatism: Microchemical evidence from ore-bearing listvenite, South Eastern Desert of Egypt, Journal of Geochemical Exploration (2012), http://dx.doi.org/10.1016/j.gexplo.2012.11.004

Table 10
Carbonate minerals disseminated in the mineralized wallrocks (mostly Fe-dolomites).

wt.%	1	2	3	4	5	6	7	8	9	10	11	12	13	14	15	16	17	18	19	20
CaO	30.42	30.17	0.03	0.06	30.87	31.06	30.83	31.81	31.58	31.94	28.42	30.53	30.50	30.29	31.00	30.92	30.26	28.82	30.86	31.17
MgO	18.45	18.91	43.71	44.05	19.34	20.63	17.28	20.74	18.79	18.83	13.88	18.67	19.13	19.42	19.80	19.30	17.56	14.82	19.70	19.18
FeO	4.61	4.96	8.12	8.58	3.90	1.96	5.30	2.70	4.46	4.31	9.46	4.51	4.05	3.61	3.44	4.13	5.85	9.10	3.74	4.50
MnO	0.25	0.10	0.15	0.13	0.25	0.02	0.20	0.08	0.33	0.56	2.70	0.19	0.17	0.15	0.16	0.09	0.32	2.35	0.16	0.22
BaO	0.01	0.00	0.00	0.01	0.00	0.03	0.07	0.02	0.03	0.07	0.00	0.01	0.02	0.03	0.06	0.00	0.04	0.00	0.00	0.02
SrO	0.35	0.10	0.00	0.00	0.15	0.15	0.21	0.18	0.09	0.12	0.02	0.12	0.13	0.14	0.15	0.15	1.08	0.03	0.17	0.11
Total	54.09	54.24	52.01	52.83	54.51	53.85	53.89	55.53	55.28	55.83	54.48	54.03	54.00	53.64	54.61	54.59	55.11	55.12	54.63	55.20
Structural formula calculated basis on 2 cations																				
Ca	1.12	1.11	0.00	0.00	1.13	1.15	1.14	1.15	1.14	1.14	1.04	1.13	1.13	1.13	1.14	1.13	1.10	1.05	1.13	1.13
Mg	0.68	0.70	1.68	1.67	0.71	0.77	0.64	0.75	0.68	0.67	0.51	0.69	0.71	0.72	0.73	0.71	0.64	0.54	0.72	0.69
Fe	0.17	0.18	0.31	0.32	0.14	0.07	0.20	0.10	0.16	0.15	0.35	0.17	0.15	0.13	0.13	0.15	0.21	0.33	0.14	0.16
Mn	0.01	0.00	0.01	0.00	0.01	0.00	0.01	0.00	0.01	0.02	0.10	0.01	0.00	0.00	0.00	0.00	0.00	0.00	0.00	0.00
Ba	0.00	0.00	0.00	0.00	0.00	0.00	0.00	0.00	0.00	0.00	0.00	0.00	0.00	0.00	0.00	0.00	0.00	0.00	0.00	0.00
Sr	0.01	0.00	0.00	0.00	0.01	0.01	0.01	0.01	0.00	0.00	0.00	0.00	0.00	0.00	0.00	0.00	0.00	0.00	0.00	0.00
Total	2.00	2.00	2.00	2.00	2.00	2.00	2.00	2.00	2.00	2.00	2.00	2.00	2.00	2.00	2.00	2.00	2.00	2.00	2.00	2.00
mol%																				
$MgCO_3$	0.00	0.00	0.00	0.00	0.00	0.00	0.00	0.00	0.00	0.00	0.00	0.00	0.00	0.00	0.00	0.00	0.00	0.00	0.00	0.00
CaCO	12.48	11.25	0.06	0.09	13.26	15.36	14.42	14.57	14.25	14.42	4.33	13.01	12.96	12.94	13.53	13.28	9.82	4.57	12.98	12.93
$CaMg(CO_3)_2$	68.22	69.73	84.04	83.38	70.96	76.62	64.13	74.70	67.98	67.45	50.95	69.11	70.85	72.41	72.51	70.71	67.73	53.77	72.12	69.49
$CaFe(CO_3)_2$	17.05	18.29	15.61	16.24	14.31	7.28	19.67	9.72	16.14	15.44	34.73	16.69	15.00	13.46	12.60	15.13	21.23	33.02	13.69	16.30
$CaMn(CO_3)_2$	0.92	0.37	0.29	0.25	0.92	0.07	0.74	0.29	1.19	2.01	9.91	0.70	0.63	0.56	0.59	0.33	1.16	8.53	0.59	0.80
$BaCO_3$	0.04	0.00	0.00	0.04	0.00	0.11	0.26	0.07	0.11	0.25	0.00	0.04	0.07	0.11	0.22	0.00	0.15	0.00	0.00	0.07
$SrCO_3$	1.29	0.37	0.00	0.00	0.55	0.56	0.78	0.65	0.33	0.43	0.07	0.44	0.48	0.52	0.55	0.55	3.92	0.11	0.62	0.40
Total	100.00	100.00	100.00	100.00	100.00	100.00	100.00	100.00	100.00	100.00	100.00	100.00	99.44	99.37	99.23	99.45	99.94	99.89	99.38	99.53
Fe#	0.20	0.21	0.16	0.16	0.17	0.09	0.23	0.12	0.19	0.19	0.41	0.19	0.17	0.16	0.15	0.18	0.25	0.38	0.16	0.19
mg#	0.79	0.79	0.84	0.83	0.82	0.91	0.76	0.88	0.80	0.79	0.53	0.80	0.82	0.84	0.85	0.82	0.74	0.56	0.83	0.80

and little quartz and magnesite at the block boundaries (e.g., Frost, 1985). Precipitation of sulfides during the serpentinization and metasomatic alteration requires high fO_2 as well as high fS_2 (Frost, 1985). Changes in the pH and temperature of the fluid can lead to temporal and/or spatial phase differentiations in the alteration assemblage. Silica solubility increases in the high pH and high temperature environments, thus the fluid input that caused the formation of silica must have had a lower pH and temperature during interaction with the wall-rock (e.g., Akbulut et al., 2006). On the other hand, absence of silica indicates a higher pH and moderate to high temperature fluid (Ash et al., 1991; Uçurum, 2000), which holds the silica in solution and generates carbonate precipitation.

A maximum temperature range between 350 and 400 °C is suggested for a stable quartz-dolomite assemblage at X_{CO2} values varying between 0.1 and 0.5 at 1 kbar (Auclair et al., 1993; Weir and Kerrick, 1987). Also, Spiridonov (1991) determined a formation temperature ranging between 280 and 340 °C in CO_2-rich fluid inclusions in larger quartz grains of the listvenite-like metasomatites from Zod gold deposit (Armenia). In the Eastern Metals Ni-Cu-Zn deposits (Quebec Appalachians), Auclair et al. (1993) suggested that Ca, CO_2, S and As-rich solutions with low fO_2, fS_2 and high temperatures (>350 °C) were necessary for carbonatization, while solutions with high fO_2 and fS_2 and moderate to low temperatures caused silicification of the wallrock.

The pyrite-arsenopyrite-pyrrhotite assemblage, together with the As at.% in arsenopyrite allows the use of fS_2- and temperature-dependent stability fields (Fig. 5) at 1 bar of Toulmin and Barton (1964) and Barton (1969). Estimated formation conditions of this assemblage in the Haimur gold deposit are $fS_2 = -8$ and $T = 350$–400 °C, consistent with the alteration assemblage and presence of Co-gersdorffite. Conditions of formation of the Haimur Cr-chlorite, talc, serpentine, sulfarsenides and sulfides are restricted to the lower $fO2$, higher Σ_S part of the serpentine–talc–magnesite field (i.e., close to the pyrite–pyrrhotite–magnetite triple point at fO_2 of around −30 (cf. Frost, 1985). This value is slightly above the quartz–fayalite–magnetite (QFM) buffer and below the Ni–NiO buffer, typical for orogenic lode gold deposits (e.g., Huston and Large, 1989).

7. Conclusions

Gold-bearing quartz veins are confined to listvenite zones in Haimur gold deposit. Textural relationships of fuchsite, Cr-chlorite and relicts of Cr-spinel crystals indicate that these Cr mobilization from primary Cr-spinels through metasomatism. Based on the electron microprobe data, positive correlations between Ni, As, Cu and Au in the late pyrite–arsenopyrite–chalcopyrite association and variable contents of Cr_2O_3 in chlorite and fuchsite reflect gold and other elements mobilization during listvenitization.

The estimated formation conditions of Haimur gold deposit are $fS_2 = 10^{-8}$ and fO_2 of around 10^{-30}, while the system cooled down from above 400 to less than 250 °C. These temperature ranges, along with the estimated sulfur and oxygen fugacities correlate well with the pervasively silicified ore-bearing listvenite, genetically linked with greenschist facies metamorphism. The chemical composition of the hydrothermal phases associated with disseminated sulfide-sulfarsenides reflects high a_{CO2} and variable $a_{Na/K}$ of the hydrothermal fluid.

These results encourage a detailed exploration program on the ophiolitic blocks associated with major fault zones in the Eastern Desert of Egypt in an attempt to vectoring to potential ore-bearing listvenites. Integrated with comprehensive petrographic studies, tracing the dispersion of Cr, Ni and Au in zones of highly tectonized ophiolites would efficiently be used to identify subtle mineralizations.

Acknowledgment

This work is financed by the Egyptian Science and Technology Development Fund (STDF), grant no. 150. We highly acknowledge the immense encouragement by the STDF team. Thanks should go to Prof. Dr. B. Lehmann, Prof. Dr. P. Weihed and colleagues from Benha Univ. Comments by the associate editor, David Huston and anonymous reviewers greatly added to the early version of this manuscript.

References

Abd El-Naby, H.H., Frisch, W., 2002. Origin of the Wadi Haimur–Abu Swayel gneiss belt, south Eastern Desert, Egypt: petrological and geochronological constraints. Precambrian Research 113, 307–322.
Akbulut, M., Pişkin, Ö., Karayiğit, A.I., 2006. The genesis of the carbonatized and silicified ultramafics known as listvenites: a case study from the Mihalýççýk region (Eskis, ehir), NW Turkey. Geological Journal 41, 557–580.
Ash, C.H., Macdonald, R.W.J., Arksey, R.L., 1991. Towards a Deposit Model for Ophiolite Related Mesothermal Gold in British Columbia. Geological Fieldwork 1991, British Columbia Department of Energy and Mines, Paper 1992–1, pp. 253–260.
Auclair, M., Gauthier, M., Trottier, J., Je´brak, M., Chartrand, F., 1993. Mineralogy, geochemistry, and paragenesis of the eastern metals serpentinite-associated Ni-Cu-Zn deposit, Quebec Appalachians. Economic Geology 88, 123–138.
Balyiss, P., 1982. A further crystal structure refinement of gersdorffite. American Mineralogist 67, 1058–1064.
Barnes, S.J., 2000. Chromite in komatiites, II Modification during greenschist to mid-amphibolite facies metamorphism. Journal of Petrology 41, 387–409.
Barnes, S.J., Roeder, P.L., 2001. The range of spinel compositions in terrestrial mafic and ultramafic rocks. Journal of Petrology 42, 2279–2302.
Barton Jr., P.B., 1969. Thermochemical study of the system Fe–As–S. Geochimica et Cosmochimica Acta 33, 841–857.
Boschi, C., Dini, A., Dallai, L., Ruggieri, G., Gianelli, G., 2009. Enhanced CO_2-mineral sequestration by cyclic hydraulic fracturing and Si-rich fluid infiltration into serpentinites at Malentrata (Tuscany, Italy). Chemical Geology 265, 209–226.
Botros, N.S., 1993. The possible occurrence of placer gold in areas lacking quartz veins in Egypt. Journal of Geochemical Exploration 49, 287–290.
Buisson, G., Leblanc, M., 1985. Gold in carbonatized ultramafic rocks from ophiolite complexes. Economic Geology 80, 2026–2029.
Buisson, G., Leblanc, M., 1987. Gold in mantle peridotites from Upper Proterozoic ophiolites in Arabia, Mali, and Morocco. Economic Geology 82, 2091–2097.
El-Dougdoug, A., 1990. Gold anomalies in the Late Proterozoic felsic/mafic volcanosedimentary sequence and associated rocks, Gebel Abu Marawat area, Eastern Desert, Egypt. Bulletin of the Faculty of Science, Cairo University 58, 533–548.
El-Mezayen, A.M., Hassaan, M.M., El-Hadad, M., Hassanein, M.M., 1995. Petrography, geochemistry and ore microscopy of Abu Marawat metavolcanics and associated gold mineralisation, North Eastern Desert, Egypt. Bulletin of the Faculty of Science, Al-Azhar University 6 (2), 1999–2021.
El Nisr, S.A., 1997. Late Precambrian volcanism at Wadi Allaqi, SE Desert, Egypt: evidence for continental arc/continental margin environment. Journal of African Earth Sciences 24, 301–313.
El-Shimi, K.A., 1996. Geology, structure and exploration of gold mineralization in Wadi Allaqi area (SW, Eastern Desert, Egypt). Ph.D. Thesis, Ain Shams University, Egypt, 326 pp.
Fleet, M.E., Mumin, A.H., 1997. Gold-bearing arsenian pyrite and marcasite and arsenopyrite from Carlin Trend gold deposits and laboratory synthesis. American Mineralogist 82, 182–193.
Frimmel, H.E., 1997. Chlorite thermometry in the Witwatersrand Basin: constrains on the Paleoproterozoic geotherm in the Kaapvaal Craton, South Africa. Journal of Geology (Chicago) 105, 601–615.
Frost, B.R., 1985. On the stability of sulphides, oxides and native metals in serpentinite. Journal of Petrology 26, 31–63.
Gabra, S.Z., 1986. Gold in Egypt. A commodity package: minerals, petroleum and groundwater assessment program. USAID project 363–0105. Geological Survey of Egypt (86 pp.).
Groves, D.I., Keays, R.R., 1979. Mobilization of ore-forming elements during alteration of dunites, Mt. Keith-Betheno, Western Australia. The Canadian Mineralogist 17, 373–389.
Halls, C., Zhao, R., 1995. Listvenite and related rocks: perspectives on terminology and mineralogy with reference to an occurrence at Cregganbaun, Co. Mayo, Republic of Ireland. Mineralium Deposita 30, 303–313.
Hansen, L.D., Dipple, G.M., Gordon, T.M., Kellet, D.A., 2005. Carbonated serpentinite (Listwanite) at Atlin, British Columbia: a geological analogue to carbon dioxide sequestration. The Canadian Mineralogist 43, 225–239.
Hassaan, M.M., El Mezayen, A.M., Dardir, A.A., Hassanein, M.M., 1996. Primary distribution pattern of gold and associated elements in Abu Marawat mine, North Eastern Desert and significance to exploration. Al-Azhar Bulletin of Science 7 (1), 995–1016.
Hassaan, M.M., Ramadan, T.M., Abu El Leil, I., Sakr, S.M., 2009. Lithochemical surveys for ore metals in arid region, Central Eastern Desert, Egypt: using Landsat ETM+ imagery. Australian Journal of Basic and Applied Sciences 3, 512–528.
Huston, D.L., Large, R.R., 1989. A chemical model for the concentration of gold in volcanogenic massive sulfide deposits. Ore Geology Reviews 4, 171–200.
Johannes, W., 1969. An experimental investigation of the system $MgO–SiO_2–H_2O–CO_2$. American Journal of Science 267, 1083–1104.
Klemm, D.D., 1965. Syntheses und Analysen in den Dreiecksdiagrammen FeAsS–CoAsS–NiAsS und $FeS_2–CoS_2–NiS_2$. Neues Jahrbuch fur Mineralogie Abhandlungen 103, 205–255.

Please cite this article as: Emam, A., Zoheir, B., Au and Cr mobilization through metasomatism: Microchemical evidence from ore-bearing listvenite, South Eastern Desert of Egypt, Journal of Geochemical Exploration (2012), http://dx.doi.org/10.1016/j.gexplo.2012.11.004

Klemm, D.D., Klemm, R., Murr, A., 2001. Gold of the Pharaohs — 6000 years of gold mining in Egypt and Nubia. Journal of African Earth Sciences 33, 643–659.
Kojonen, K., Johanson, B., 1999. Determination of refractory gold distribution by microanalysis, diagnostic leaching and image analysis. Mineralogy and Petrology 67, 1–19.
Kolonin, G.R., Pal'yanova, G.A., Shironosova, G.P., Morgunov, K.G., 1997. The effect of carbon dioxide on internal equilibria in the fluid during the formation of hydrothermal gold deposits. Geochemistry International 35, 40–50.
Kovalenker, V.A., Tsonev, D., Breskovska, V.V., Malov, V.C., Troneva, N.V., 1986. New Data on the Mineralogy of the Massive-Sulphide Deposits in the Central Srednogorie of Bulgaria (in Russian). Metasomatism, mineralogy and genesis of gold and silver deposits in volcanic series. Nauka, Moscow, pp. 91–110.
Kranidiotis, P., MacLean, W.H., 1987. Systematics of chlorite alteration at the Phelps Dodge massive sulfide deposit, Matagami, Quebec. Economic Geology 82, 1898–1911.
Kretschmar, U., Scott, S.D., 1976. Phase relations involving arsenopyrite in the system Fe–As–S and their application. The Canadian Mineralogist 14, 364–386.
Kusky, T.M., Ramadan, T.M., 2002. Structural controls on Neoproterozoic mineralization in the South Eastern Desert, Egypt: an integrated field, Landsat TM, and SIR-C/X SAR approach. Journal of African Earth Sciences 35, 107–121.
Leblanc, M., Fischer, W., 1990. Gold and platinum group elements in cobalt-arsenide ores: hydrothermal concentration from a serpentinite source-rock (Bou Azzer, Morocco). Mineralogy and Petrology 42, 197–209.
Likhoidov, G.G., Plyusnina, L.P., Shcheka, Zh.A., 2007. The behavior of gold during listvenitization: experimental and theoretical simulation. Doklady Earth Sciences 415 (5), 723–726.
Mellini, M., Rumori, C., Viti, C., 2005. Hydrothermally reset magmatic spinels in retrograde serpentinites, formation of "ferritchromit" rims and chlorite aureoles. Contributions to Mineralogy and Petrology 149, 266–275.
Molchanov, V.P., Zimin, S.S., Oktyabr'skii, S.A., et al., 2000. Mineral Composition and Gold Potential of Listvenites of the Ust'-Dep Ophiolite Zone in Ore Deposits of Continental Margins. Dal'nauka, Vladivostok, pp. 170–180 (in Russian).
Molchanov, V.P., Plyusnina, L.P., Khanchuk, A.I., Zimin, S.S., Oktyabr'skii, R.A., 2006. Platinum- and gold-bearing rodingites of the ust'-dep ophiolite block (middle Amur region). Doklady Earth Sciences 407 (2), 250–253.
Nekrasov, I.Ya., Samusikov, V.P., Leskova, N.V., 1988. The first finding of sulfide AgAuS, an analog of petrovskaite. Doklady Akademii Nauk 303 (4), 944–947.
Nixon, G.T., 1990. Geology and Precious Metal Potential of Mafic-Ultramafic Rocks in British Columbia: Current Progress. Geological Fieldwork 1989, Paper 1990–1, a summary of field activities and current research, province of British Columbia. Mineral Resources Division Geological Survey Branch, pp. 353–358.
Osman, A., 1995. The mode of occurrence of gold-bearing listvenite at El Barramiya gold mine, Eastern desert, Egypt. Middle East Research Centre. Ain Shams University. Earth Sciences Series 9, 93–103.
Pal'yanova, G.A., Kolonin, G.R., 2004. Physicochemical features of the behavior of gold and silver in processes of hydrothermal ore formation. Doklady Earth Sciences 394, 100–103.
Pan, Y., Fleet, M.F., 1989. Metamorphic petrology and gold mineralization of the White River gold prospect, Hemlo area, Ontario. Ontario Geological Survey, Miscellaneous Paper 143, 42–52.
Plissart, G., Féménias, O., 2009. Mineralogy and geothermometry of gabbro-derived listvenites in the Tisovita-Iuti ophiolite, south western Romania. The Canadian Mineralogist 47, 81–105.
Ramadan, T.M., 1997. Shear Zone Gold Mineralization at Marsa Sha'b area, South Eastern Desert, Egypt. Fourth Biennial SGA Meeting, Turku, Finland, pp. 293–296.
Ramadan, T.M., 2002. Exploration for gold-bearing listwaenites at Um Khasila area, Central Eastern Desert, Egypt. Egyptian Journal of Remote Sensing and Space Sciences 5, 63–76.
Ramadan, T.M., Abu El-Leil, I., Hassaan, M.M., Shalaby, I.M., 1998. Geological and Geochemical Studies on the Ophiolitic Rocks at Gebel Sirsir Area, South Eastern Desert, Egypt. International. Ophiolite Symposium, Oulu, Finland.
Ramadan, T.M., Abdelsalam, M.J., Stern, R.J., 1999. Mineral Exploration with Landsat TM and SIR-C/X SAR Images: Wadi Allaqi Suture, South Eastern Desert, Egypt. South-Central Geol. Soc. Amer. Meeting, 1, Lubbock, Texas, p. A33.
Ramadan, T.M., Sadek, M.F., Abu El Leil, I., Salem, S.M., 2005. Um El Touyur El Fuqani gold mineralization, South Eastern Desert, Egypt: using Landsat ETM+ IMAGERY. Annals of the Geological Survey of Egypt 28, 263–281.
Robinson, P.T., Malpas, J., Zhou, M.-F., Ash, C., Yang, J.-S., Bai, W.J., 2005. Geochemistry and origin of Listwanites in the Sartohay and Luobusa ophiolites, China. International Geology Review 47, 177–202.
Sazanov, V.N., 1975. Listvenitization and mineralization (Listvenitizaciya iorudeneniye) Izdatelistvo Nauka. Science Publishers, Moscow.
Spiridonov, E.M., 1991. Listvenites and zodites. International Geology Review 33, 397–407.
Toulmin, P., Barton, P.B., 1964. A thermodynamic study of pyrite and pyrrhotite. Geochimica et Cosmochimica Acta 33, 671–690.
Uçurum, A., 2000. Listwaenites in Turkey: Perspectives on formation and precious metal concentration with reference to occurrences in East–Central Anatolia. Ofioliti 25, 15–29.
Weir, R.H., Kerrick, M., 1987. Mineralogic, fluid inclusion, and stable isotope studies of several gold mines in the Mother Lode, Tuolumne and Mariposa Counties, California. Economic Geology 82, 328–344.
Wu, X., Delbove, F., 1989. Hydrothermal synthesis of gold-bearing arsenopyrite. Economic Geology 84, 2029–2032.
Ziebold, T.O., 1967. Precision and sensitivity in electron microprobe analysis. Analytical Chemistry 39, 858.
Zoheir, B.A., 2008. Characteristics and genesis of shear zone-related gold mineralization in Egypt: a case study from the Um El Tuyor mine, south Eastern Desert. Ore Geology Reviews 34, 445–470.
Zoheir, B.A., 2011. Transpressional zones in ophiolitic mélange terranes: potential exploration targets for gold in the South Eastern Desert, Egypt. Journal of Geochemical Exploration 111, 23–38.
Zoheir, B.A., Lehmann, B., 2011. Listvenite–lode association at the Barramiya gold mine, Eastern Desert, Egypt. Ore Geology Reviews 39, 101–115.

Please cite this article as: Emam, A., Zoheir, B., Au and Cr mobilization through metasomatism: Microchemical evidence from ore-bearing listvenite, South Eastern Desert of Egypt, Journal of Geochemical Exploration (2012), http://dx.doi.org/10.1016/j.gexplo.2012.11.004